



# Encapsulation of expansive powder minerals within a concentric glass capsule system for self-healing concrete



T.S. Qureshi\*, A. Kanellopoulos, A. Al-Tabbaa

Department of Engineering, University of Cambridge, Trumpington Street, Cambridge CB2 1PZ, UK

## HIGHLIGHTS

- Dry expansive minerals encapsulated in concentric glass capsule for self-healing.
- Dispersion and diffusion of healing agent from capsules triggered healing mechanisms.
- Crack bridging occurred by effective formation of healing compounds in mortar matrix.
- Very large cracks (~400  $\mu\text{m}$ ) found to be effectively healed with capsule system.

## ARTICLE INFO

### Article history:

Received 11 January 2016

Received in revised form 31 March 2016

Accepted 12 June 2016

### Keywords:

Powder mineral encapsulation

Expansion

Crack sealing

Strength recovery

Durability

Self-healing kinetics

Materials microstructure

## ABSTRACT

This study presents the application of encapsulated expansive powder minerals (magnesium oxide, bentonite and quicklime) for self-healing of cement-based mortars. A system of concentric glass macrocapsules was used to envelope the expansive minerals (outer capsule) and water (inner capsule). Mortar samples containing concentric macrocapsules with different mineral combinations were cracked and healed under three different curing regimes; ambient conditions, high humidity exposure and immersed in water. Self-healing was assessed based on visual crack sealing, mechanical strength recovery and improvement in durability investigated by means of capillary sorption tests. Micro-structural analysis of the healing materials was investigated using FT-IR, XRD and SEM-EDX for exploring self-healing kinetics. Immersed in water have yielded the optimum healing efficiency with ~95% crack sealing and ~25% strength recovery in 28 days. Data showed an increasing trend in 56 days for both crack sealing and load recovery. The improvement in terms of capillary absorption of healed samples was also significant after 28 days of healing. Self-healing kinetics revealed that the expansive minerals were hydrated in the initial healing period and slowly carbonated over time until the peripheral crack zone became adequately water tight.

© 2016 The Authors. Published by Elsevier Ltd. This is an open access article under the CC BY-NC-ND license (<http://creativecommons.org/licenses/by-nc-nd/4.0/>).

## 1. Introduction

Self-healing in concrete can be broadly classified into two categories: autogenic and autonomic healing [1]. Autogenic healing is an intrinsic material healing property which is triggered with the hydration of unhydrated cement remaining in the matrix. Early age concrete can heal naturally due to continued hydration of un-hydrated cement particles existing in the matrix. In addition, healing is also promoted by precipitation of carbonates and crystal growth especially near the crack tips. Autonomic healing on the other hand is the use of components which normally are not present in cement based composites. This category typically refers to different types of materials incorporated into the matrix usually

in the form of encapsulated additions. Self-healing is triggered upon crack formation which results in the rupture of the encapsulated system and the subsequent release of the healing compounds. The autonomic concept has been developed to tackle the limitations of autogenous healing [2–4]. These include dependence on the age of the concrete, as older concrete structures have less unhydrated cement particles, and the lack of healing larger cracks, as autogenic processes can typically heal cracks up to 150  $\mu\text{m}$  [5] at best case. Although the maximum healable crack width limit was reported widely varied between 5 to 300  $\mu\text{m}$  [3], autogenous healing crack width limit varies based on the cement content, existence of supplementary materials, water content and age.

Single-component, air-curing healing agents, such as silicon based adhesive, cyanoacrylates, epoxy and alkali-silica solutions are preferred by different researchers [6–9]. Incorporation of these single component agents inside concrete systems is rather simple

\* Corresponding author.

E-mail address: [tsq20@cam.ac.uk](mailto:tsq20@cam.ac.uk) (T.S. Qureshi).

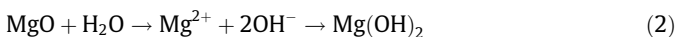
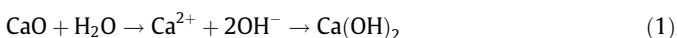
compared to incorporation of the multi-component methyl-methacrylate [10] and two-component epoxy resin [8,9] systems. However, Dry and McMillan have argued that the short shelf life of single-component healing agents might be disadvantageous and multi-component healing agents have more stability over time [10]. In contrast, having further improved shelf-life, Mihashi et al. [9] depicted the limitation of two component epoxy resins due to insufficient mixing of the components inside the crack. This had resulted poor performance compared to a single-agent cyanoacrylates type adhesive agents. Recently, Van Tittelboom et al. [11] investigated the use of a two-component polyurethane foam as healing agent. They suggested that healing agents should have a low viscosity and that the polymerization reaction should not depend on the mix ratio of the two components.

Nevertheless polymeric resins can effectively recover the mechanical properties of concrete, they have the major drawback of limited shelf life (of single component resins), effective mixing (of two component resins) and cost when used in bulk quantities. The use of minerals compatible with the cementitious materials can resolve these limitations. Few studies reported the use of sodium silicate in microcapsules for self-healing concrete [12]. However, in these studies neither many details were given on the encapsulated system nor details on the actual self-healing processes and kinetics were provided. In a recent study, the authors reported the effectiveness of encapsulated liquid SiO<sub>2</sub> precursors, sodium silicate and powder MgO as healing materials using a system of parallel thin walled glass capsules [4]. This study showed that sodium silicate and colloidal silica could improve dramatically the durability performance of cracked mortar samples. The results of the MgO powder were also promising; however, their limited healing performance was noted due to its poor dispersion in the crack plane while investigating the crack faces of the samples.

### 1.1. Concentric glass macrocapsules' system

Since the major issue reported previously [4] regarding the encapsulation of mineral powder was its proper dispersion in the crack, this study focuses on an encapsulation system that will improve powder dispersion. To achieve this, a system of concentric glass macrocapsules was adopted with the inner capsule containing water and the outer capsule containing the powder minerals (Fig. 1).

Three expansive powder minerals (MgO, bentonite, and quicklime) were used in this study. These minerals are known for their expansive properties during hydration and carbonation, and have been used previously for improving the autogenous healing capacity of a Portland cement (PC) system [13–16]. Principal products that are produced during the initial hydration of MgO and quicklime (CaO) are brucite (Mg(OH)<sub>2</sub>) and portlandite (Ca(OH)<sub>2</sub>) following the reaction in Eqs. (1) and (2) below. These hydration products have the potential to accelerate the self-healing mechanism [13,16] as they have cementing and crystal forming properties.



Bentonite is renowned for its swelling and expanding properties while bearing in contact with water. Literature further suggests that bentonite in high alkaline solutions can be modified in an aqueous silica solution and that the hydroxide solubility increases at pH > 11 [17] following the reaction refer to Eq. (3):

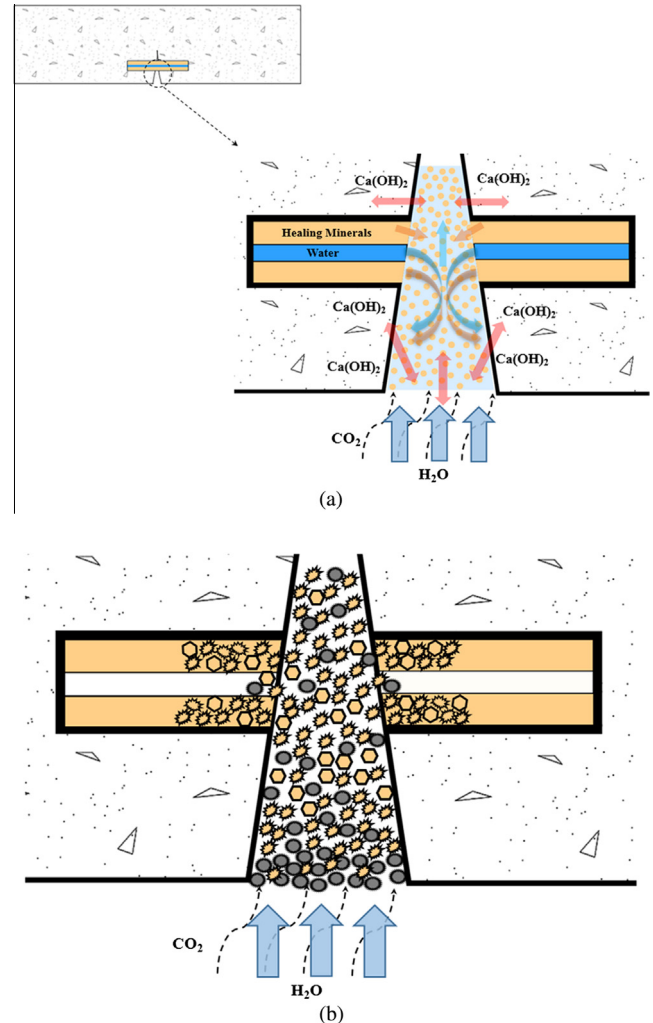
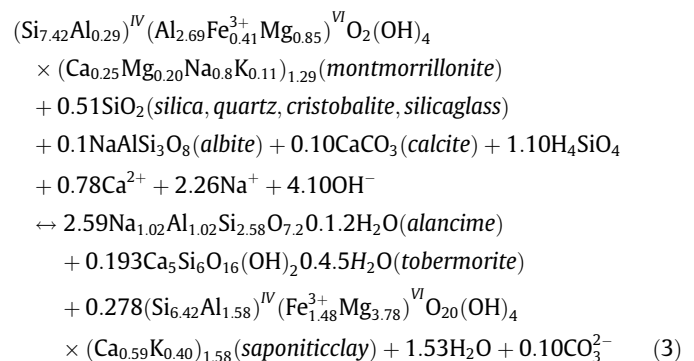


**Fig. 1.** Basic concept of the concentric glass capsules self-healing: (a) Release of expansive minerals within the cracks through dispersion and diffusion after crack formation and (b) consequent interaction of released healing agent with water and CO<sub>2</sub> results in the formation of different hydrated and carbonated products to seal and possibly heal the crack.



Sanchez et al. [17] have characterised the hyper-alkaline reaction of Na-bentonite (0.5–0.1 M) by the dissolution of montmorillonite and the precipitation of zeolites, phillipsite, saponite, calcium silicate hydrate-gel, tobermorite and gyrolite in different temperature ranges which was driven by montmorillonite dissolution. This property of bentonite makes it a suitable choice as expansive healing agent for self-healing concrete.

Research in the field of expansive minerals showed that these can improve the autogenous healing in cement-based materials [13,16]. However, once mixed as supplementary materials in concrete they do partially react with the hydration products and the water present in the cement based compound. Therefore, their potential for self-healing is somewhat reduced. By encapsulating the powder minerals, they are protected from the rest of the constituents of the mix thus more efficient self-healing performance is expected compared to previously reported autogenous self-healing systems. The advantages of the proposed system can be attributed to (i) the release of healing minerals when they are needed, in other words just after damage occurs and (ii) spreading of the minerals into the cracks through dispersion and diffusion.

### 1.2. Potential stages in the proposed self-healing kinetics

The hydration kinetics for self-healing are similar to cement hydration as reported in [18] and involve several processes. The self-healing kinetics may occur either in consecutive order, or simultaneously, or in combination of two or more of the stages below:

1. Dispersion of minerals from the encapsulation systems into the crack surface.
2. Dissolution of the unhydrated cracked surface and dispersed healing minerals. In this stage solid minerals from the surface and capsule come in contact with water leading to detachment of molecular units for initial hydration reactions [19]. Minerals continue to dissolve until a maximum ionic saturation level is reached in the aqueous mineral solution.
3. The adsorption stage involves the ions or other molecular units accumulation at an interface [20], for example the solid particle surface in a liquid.
4. The nucleation stage involves homogenous or heterogeneous precipitation of solids into the solution. According to Kashchiev and Rosmalen [21] this stage is reached when the bulk free energy driving force for forming the solid is greater than the atomic energy required for the hydration reaction in forming the new solid-liquid interface. This is the key stage for the initiation of the hydration reaction.
5. The growth stage is the process of molecular units' incorporation into the amorphous solid or a crystalline structure [22] as its self-adsorption layer. In this stage, hydration products start to form a solid structure from the powder and the liquid.
6. Complexation is the adsorption of available seed ions into a complex on solid surfaces [23]. It is a transmission reaction process of ions to accumulate to a complex mix production. This triggers the formation of multi-component hydration products such as calcium silicate hydrates.
7. The diffusion control stage initiates the transportation of dissolved components through the solid crack surface of the cement mortar matrix in the adsorption layers. An in-depth analysis of the diffusion kinetics could be found in [20]. Unhydrated minerals from the encapsulation systems at the later stage may be transported to the crack zone through diffusion.







## 2. Materials and sample preparation

### 2.1. Materials and test series

Table 1 summarises the test series and associated encapsulated mineral agents used in this study. In this table, PC is CEM I 52.5 N according to BS EN 197-1. Reactive MgO (92/200) was supplied by RBH Ltd, China with the reactivity of 145 s following the acidic reactivity testing process of [24,25]. Bentonite was supplied by Kentish minerals and Quicklime (Calbux) according to BS EN

**Table 1**

Test series used to compare the self-healing glass tube systems.

Code	Minerals (mm)	Encapsulation geometry	Healing conditions		
			Immersed	High-humid	Ambient
CON	–	No tube	✓		✓
MD	MgO		✓	✓	✓
PC-D	PC		✓	✓	✓
BD	Bentonite		✓	✓	✓
QD	Quicklime		✓	✓	✓
OPT-D	MgO, CaO and bentonite		✓	✓	✓
SHC-D	PC with MgO, CaO and bentonite		✓	✓	✓

459-1:2001 was supplied by Tarmac Buxten Lime and Cement, UK. Further details of the used expansive minerals (MgO, bentonite and quicklime) can be found in [13,16]. Mineral and water containing capsules were embedded into mortar (1.5:1 sand to cement ratio) prism samples. Fine sand, sourced locally, was used for the production of mortar mixes with  $D_{50}$  of 0.85 mm and a coefficient of uniformity about 4.3.

In Table 1, OPT-D refers to an optimum combination that consists of only expansive minerals (40%MgO, 40%CaO and 20% bentonite), and SHC-D refers to a self-healing cement combination that consists of 87.5% PC with 5%MgO, 5% CaO and 2.5% bentonite. These optimum mineral combinations were composed based on the efficient healing trend obtained in our previous [13] and on going study, and further advancement is submitted for publication elsewhere.

### 2.2. Encapsulation system, sample preparation and curing

The different combinations of expansive minerals, as stated in Table 1, were encapsulated by thin-walled concentric glass capsules (Fig. 2) where the minerals were contained in the outer capsule and the capsule in the core carried the water. The wall thickness of both capsules was 0.45 mm and their internal diameters were 11.4 mm and 6.15 mm for the outer and inner capsule respectively. The length of the encapsulating system was 50 mm. The glass capsules were filled and sealed and their sealing was checked following the procedure described in [4]. Once prepared, the concentric capsule system was positioned in the middle of mortar prisms (50 mm × 50 mm × 220 mm) with a mortar cover of 7.5 mm from the bottom face (Fig. 2b). One concentric capsule per prism was used. A 1.6 mm in diameter mild steel tie wire was placed at the top of the prism samples (above neutral axis with 10 mm mortar cover from top surface) to avoid brittle failure during loading and re-loading and thus allowing control of the crack opening (Fig. 2c). The mortar preparation, sample casting and seven day curing in water before initial cracking procedure were same as described in [4].

## 3. Experimental methods

### 3.1. Mechanical loading and healing efficiency

Prior to cracking, the prism samples were notched with a rotating diamond blade. The notch depth and width were 1.5 and 2.0 mm respectively. Then the samples were cracked under three-point bend test using a 30 kN static loading frame (Fig. 3). The distance between the supports amounted to 150 mm. The load was increased with a rate of 0.125 mm/min. The crack width was

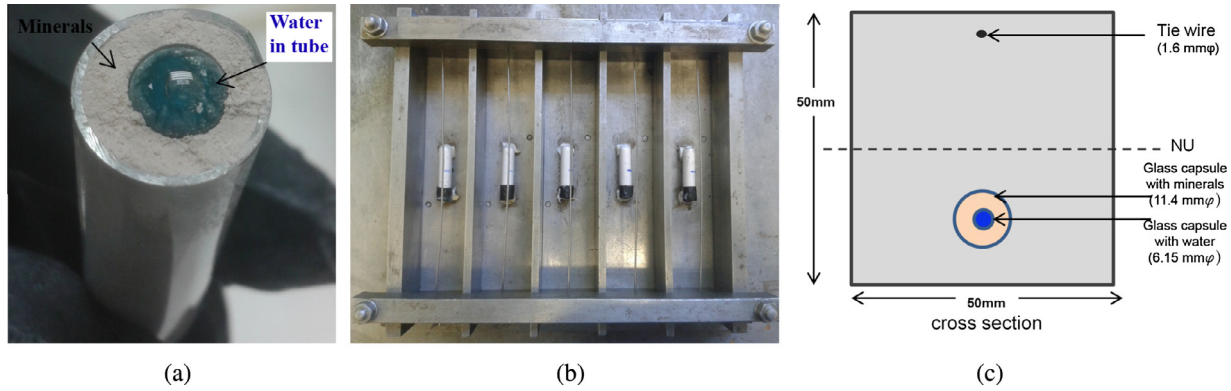


**Fig. 2.** a. Expansive minerals and water in double tube glass capsules. b. Glass capsules attached at the bottom of the prism moulds. c. Cross-section of the prism samples experimental setup.

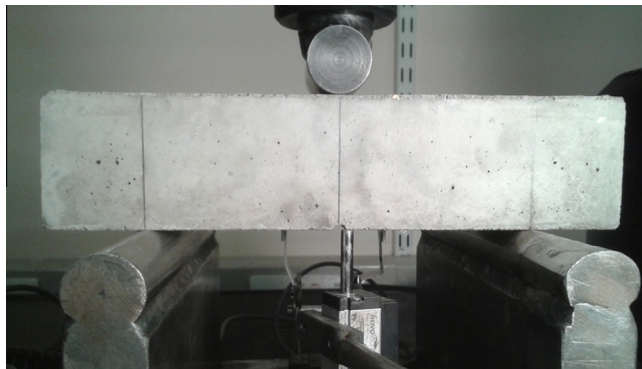


**Fig. 3.** Three-point bending experimental set-up for cracking the notched mortar prisms.

controlled using a clip gauge and the loading was halted when cracks were opened to 0.40–0.50 mm allowing the glass capsule to rupture and to release the healing agent. Upon load removal each series of specimens had an average residual within a range of 0.36–0.38 mm.

Cracked samples were then left to heal under three different curing conditions (ambient, immersed, and high humidity) for a period of 28 days and 56 days. The temperature was kept constant at  $20 \pm 1$  °C in all three healing regimes. High humidity samples were placed in sealed boxes with relative humidity >90%. The samples were exposed to their curing conditions immediately after cracking. Samples were re-loaded after healing and the load recovery rate coefficient (LR%) was calculated in each case following Eq. 4 below:

$$LR(\%) = \frac{P_{max,h} - P_{un}}{P_{max,i} - P_{un}} \times 100 \quad (4)$$

where  $P_{max,i}$  (N) is the load at which initial cracking occurred,  $P_{un}$  (N) is the unloading point of the first test and  $P_{max,h}$  (N) is the maximum load attained by the healed sample during reloading.

### 3.2. Healing characterisation

#### 3.2.1. Crack area measurements

The cracks were marked at the bottom (3 spots) and the side (2 spots) faces of the prisms and subsequent sealing was monitored using a stereoscope over time. Each time images were taken at the exact same locations in order to have a meaningful comparison. The side spots were measured on both of the sides. Image analysis software with inbuilt algorithms (Image-J) was then used

to measure the crack-section and the crack area reduction percentage (CA%) was calculated for comparison. The CA (%) was calculated using Eq. (5):

$$CA(\%) = \frac{CA_0 - CA_t}{CA_0} \times 100 \quad (5)$$

where  $CA_0$  (mm<sup>2</sup>) is the crack cross-section area just after cracking and  $CA_t$  (mm<sup>2</sup>) is the crack cross-section area after healing time  $t$ .

#### 3.2.2. Micro-structural investigation of the healing materials

Healing materials were extracted carefully from the prism crack planes after they were reloaded. Healing compounds were investigated using Fourier transform infrared spectroscopy (FTIR), X-ray diffraction analysis (XRD) and high definition scanning electron microscopy (SEM), backscattered and EDX (Nova nano SEM 450). The EDX detector was a Bruker QUANTAX EDX, Xflash 6|100. Samples for SEM-EDX were collected carefully, while samples for FT-IR and XRD were collected using a file and a scaler tool and afterwards they were grinded (passing sieve size 75  $\mu$ m). All samples were immersed in acetone for three days immediately after collection to stop further hydration and then they were dried under vacuum for four days and in the oven (60 °C) for three more days prior to performing the test. The SEM-EDX samples were attached to the stub using carbon tape. Then a silver patching was attached around the side of samples to make them more conductive for efficient quantification. Samples were then gold coated using a K550 Emitech coating machine. These tests were conducted to characterise the developed healing materials and investigate their possible formation kinetics.

#### 3.3. Healing efficiency: liquid capillary absorption coefficient as durability indicator

A simple short-term one dimensional sorptivity test was performed following RILEM guidelines [26]. The test was performed on a set of three prisms healed for 28 days in immersed condition after breakage. Liquid uptake was measured only for the crack region so that the efficiency of the healing process was directly evaluated. Hence, the bottom of the prisms was coated with sealing adhesive aluminium tape, leaving only the crack face exposed for capillary suction. The area exposed to water during the absorption test was  $\sim 50$  mm<sup>2</sup>.

The sorptivity (liquid capillary absorption coefficient) was obtained using Eq. (6):

$$M_w = S\sqrt{t} \quad (6)$$

where  $M_w$  the water suction quantity per unit area is proportional to the square root of absorption time  $t$  (min) and  $S$  (mm/ $\sqrt{\text{min}}$ ) is

the sorptivity coefficient of concrete which is the slope between  $M_w$  and the square root of time. For all testing procedures performed in this study triplicate samples were used.

## 4. Results and discussion

### 4.1. Crack sealing efficiency and recovery of mechanical strength

The maximum load prior to cracking was followed by two distinctive sounds of breakage during the first three-point bending test. These sounds confirmed the rupture of the double glass capsules inside the prisms. Water dispersion from the tubes was observed in most cases at the side and bottom of the prisms.

The need for water to obtain crack healing was evident as the healing materials proliferation in the sample exposed to the immersed curing condition was much higher compared to the samples exposed to high humidity and ambient curing conditions. The crack sealing efficiency (CA%) under the three different curing conditions over 28 and 56 days are illustrated in Fig. 4.

Crack sealing efficiency i.e. crack opening area reduction over time was found to increase from 28 days to 56 days in similar trends. Samples with capsules healed under water resulted over 90% sealing efficiency in 28 days and over 95% in 56 days. Although bentonite capsule samples (BD) showed the lowest crack sealing of all minerals investigated (80 ~ 85%) in 28–56 days, it was still higher than the control mortar specimens (68% ~ 75%). Typical successful crack sealing patterns over time for the immersed curing condition is presented in Fig. 5.

However less prominent sealing was observed in the samples stored at ambient and high humidity conditions, where comparatively improved sealing was obtained at high humidity conditions. In ambient and high humidity, PC-D and BD capsules resulted in similar sealing performance as the CON samples, where MD, MQ, OPT-D and SHC-D show 1.5 ~ 2.5 times more efficiency compared to CON. This could be attributing to the higher water demand of PC and bentonite for producing sealing compounds. Although capsules water disperses the dry minerals initially, more water was required for the diffusion of the minerals at later stage to accelerate the hydration of minerals in the crack zone thus producing healing compounds. Hence overall the crack sealing efficiency trend was found to be SHC-D  $\geq$  PC-D  $\geq$  QD > MD  $\geq$  OPT-D > BD > CON.

Healing in immersed condition was found most efficient (Fig. 5). This response was similar to our previous findings [4] and showed the importance of water in the development of healing materials regardless the state of the mineral precursor used (liquid or powder). For the samples healed under water, considerable numbers

of cracks around ~ 400  $\mu$ m width were completely sealed within 14 days (Fig. 5 eg. PC-D and OPT-D, SHC-D). Fig. 6 shows the CA% rate for all samples at different curing times. Here BD samples showed a slow crack area reduction initially up to 14 days, while PC-D and SHC-D showed ~85% sealing.

According to Fig. 6, considerable crack sealing improving trend for QD and OPT-D were found within 14–21 days. The trend for BD samples alters after 14 days. Similar although improved, performance was noted for MD samples while they have showed significant improvement within 21–28 days. Bentonite diffusion within the crack zone was not less efficient but less crystals were formed compared to the other expansive minerals. Initially bentonite may have transported active ions in the crack faces which kept reacting gradually. Except for the CON samples, all capsule containing samples sealing kept improving in much faster rate from 14 to 28 to 56 days.

When investigating the mechanical strength recovery of the healed specimens, recovery values reflected similar trends as crack sealing efficiency except for PC-D and QD samples recovery. Load recovery (LR%) at 28 and 56 days is shown in Fig. 7. Yet again the importance of water for efficient load recovery was reflected by the results. However, some load recovery was evident in ambient and high humidity conditions as well. This was due to the dispersion of the healing minerals with water in the crack just after breaking of the capsules. Moreover, minerals inside the tubular capsules were found hydrated and hardened over time. Hardened capsules acted as a bridge between cracks thus actuating considerable mechanical strength recovery, although sealing was not efficient in ambient and high humidity conditions.

Prisms were broken completely during reloading and it was noted that cracks re-opened at the same positions. Mechanical recovery was much improved in capsule containing prisms compared to control, where combined mineral capsules resulted in a higher recovery trend at 28 days and 56 days compared to individual mineral capsules. The recovery trend was found as SHC-D > OPT-D > PC-D > MD > QD > BD with the recovery ranged from 7% for BD to 25% for SHC-D, while CON samples recovered ~4% at 28 days. Although quicklime in QD showed efficient sealing, it was not such a case in the load recovery. This could be due to quicklime's prime hydration product portlandite, which is the most efficient calcite crystal producing agent compared to other minerals in individual action. This higher proportion of crystal forming property of quicklime combining with swelling bentonite, expansive MgO and PC have resulted highest recovery in SHC-D up to 28% at 56 days.

It is known that blends containing MgO and bentonite have increased water requirements compared to standard PC mixtures [13]. This was evident in the recovery results towards ambient to

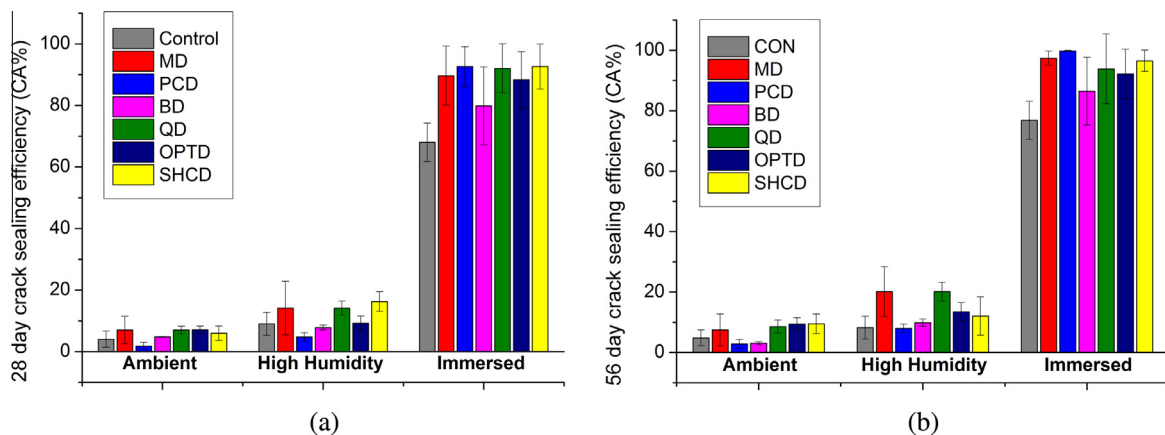


Fig. 4. Percentage reduction of the total crack area due to healing in the three different curing conditions; (a) after 28 days of healing; (b) after 56 days of healing.

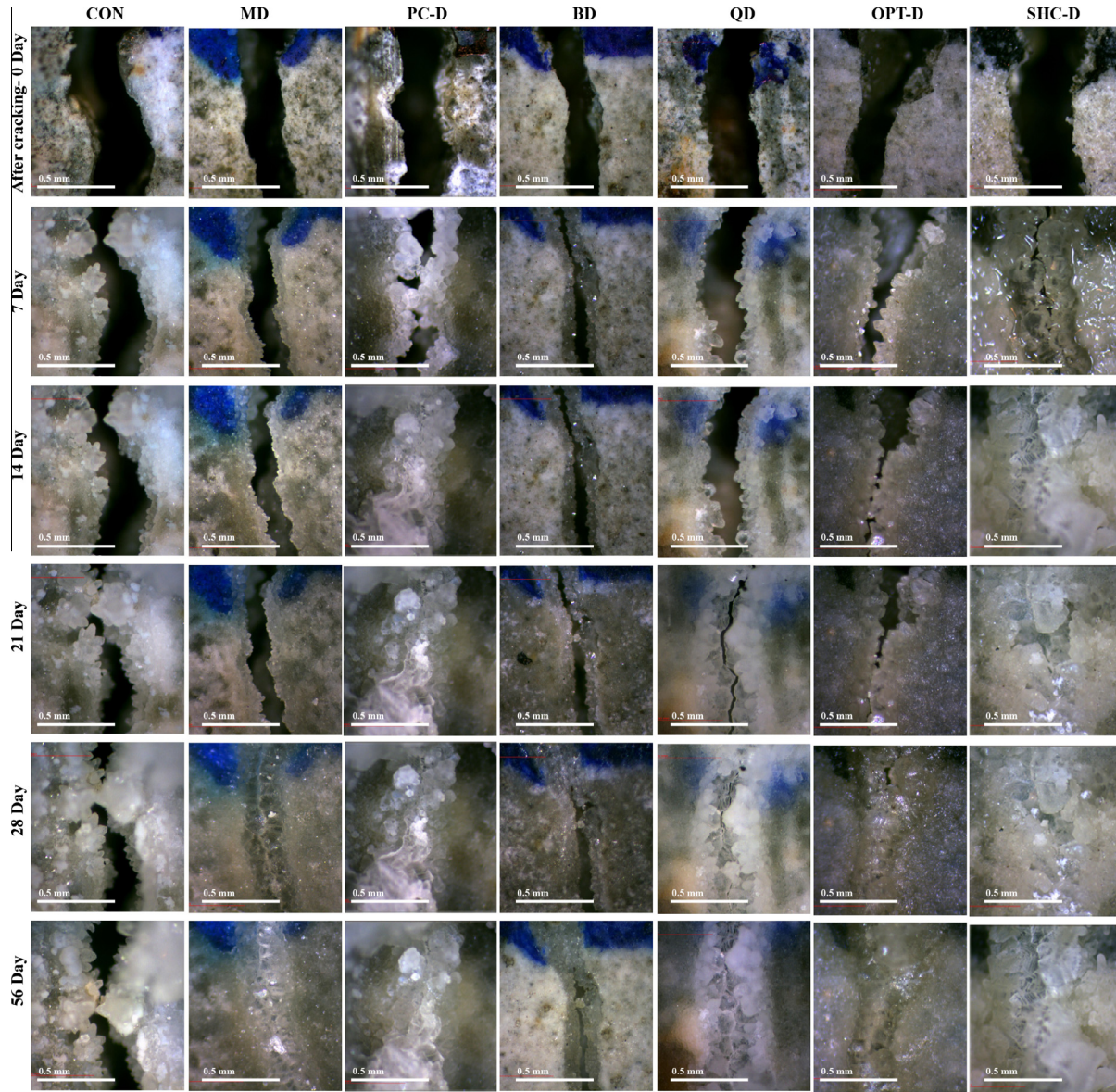


Fig. 5. Representative image of efficient crack sealing patterns over time in the immersed curing condition under digital microscope investigation.

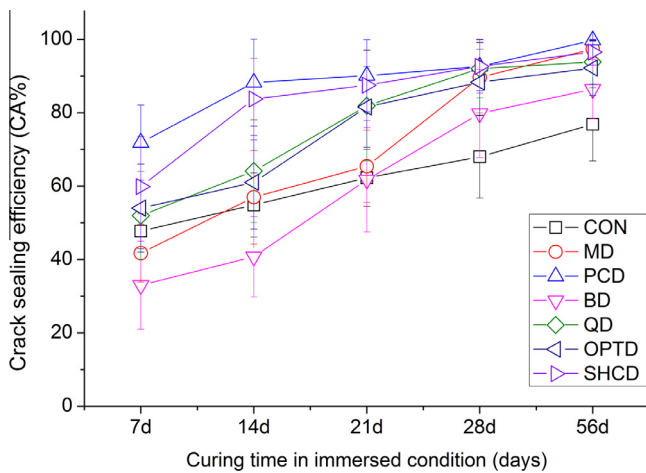
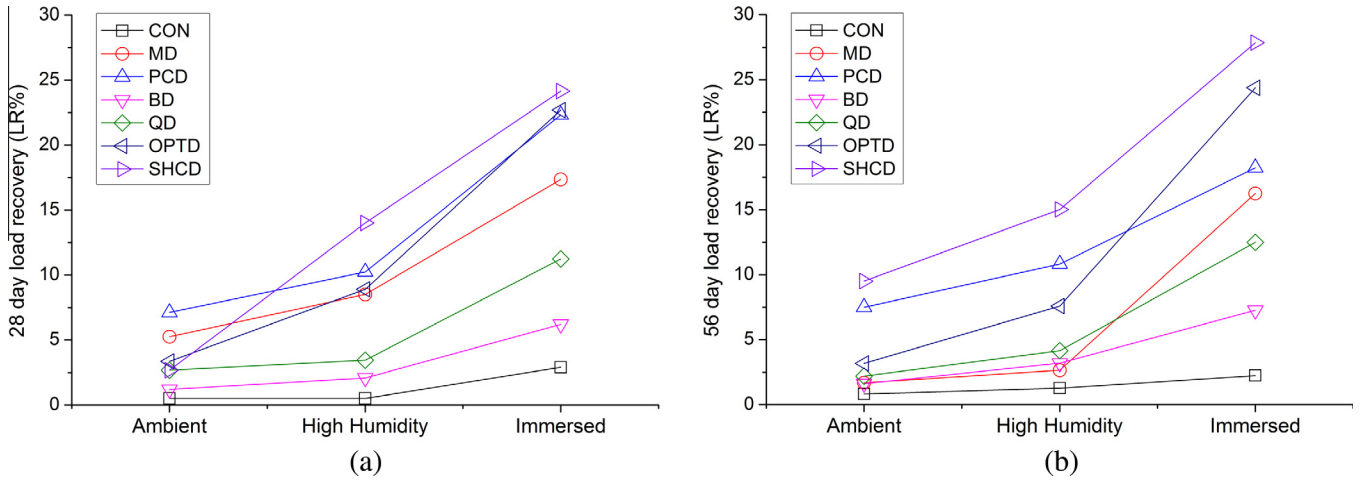


Fig. 6. Crack sealing progression over time in immersed condition.

immersed curing condition. Water requirement of MgO and bentonite was further reflected on OPT-D and SHC-D recovery results (see Fig. 7). Where SHC-D showed higher recovery compared to OPT-D in high humidity condition. Load recovery in high humidity condition was also higher compared to the previous results of liquid glass capsule system in previous study [4]. This was due to the improved glass capsule system, which efficiently dispersed the minerals in the crack instantly and with time through the continuous hydration of the capsule minerals which act as a bridge between the cracks. Overall strength recovery improved from 28 days to 56 days where SHC-D and OPT-D samples showed better stability and recovery compared to PC-D over time. Since the self-healing mechanism was dominated in immersed in water condition, the healing products analysis as well as the study of the durability indicators was focused on those samples.

#### 4.2. Characterisation of the formed self-healing materials

Minerals released from the glass tube systems initially spread through dispersion and later through diffusion process. There spreading were found most efficient in immersed condition, as dif-



**Fig. 7.** Mechanical load recovery percentage under three-point bending test for all mineral healing compound containing samples in three different curing conditions: (a) 28 days; (b) 56 days.

fusion process requires water penetration inside the crack zone. Released minerals from the encapsulation started hydrating initially after crack formation and the healing materials were precipitating with the progress of time. Carbonate rich self-healing products in particular calcite, and calcite mixed with other hydration compounds, accumulated at the air/water interface cross-section of the crack zone which were visually identified as superficial healing materials (Fig. 8).

Gradual minerals proliferation (as monitored with digital microscope) was observed in all samples (Fig. 5) and this near surface healing compounds were typically noticed in the periphery of the crack-section (Fig. 8). This over time keeps improving the water tightness and had an impact on durability. Superficial sealing crystal typical morphology for all samples were presented in Fig. 9.

These images suggest that minerals dispersed from the capsules in the crack zone had influenced the peripheral crystal formation. Typical calcite crystals were found in control samples. Inter-

grown sphere crystals forms in MD samples, where flakelike cluster of inter-grown crystals was noted in PC-D samples. Crystals of BD results layered face with clusters of pear shaped crystals and quicklime affects the formation of rhombohedral with rounded edges in QD samples. In comparison with others, OPT-D and SHC-D sealing crystals were formed in combined shapes with larger crystal structures. The observed efficient crystal formation in



**Fig. 8.** Typical self-healing materials formation pattern in the cracked cross-section of sample cured under water.

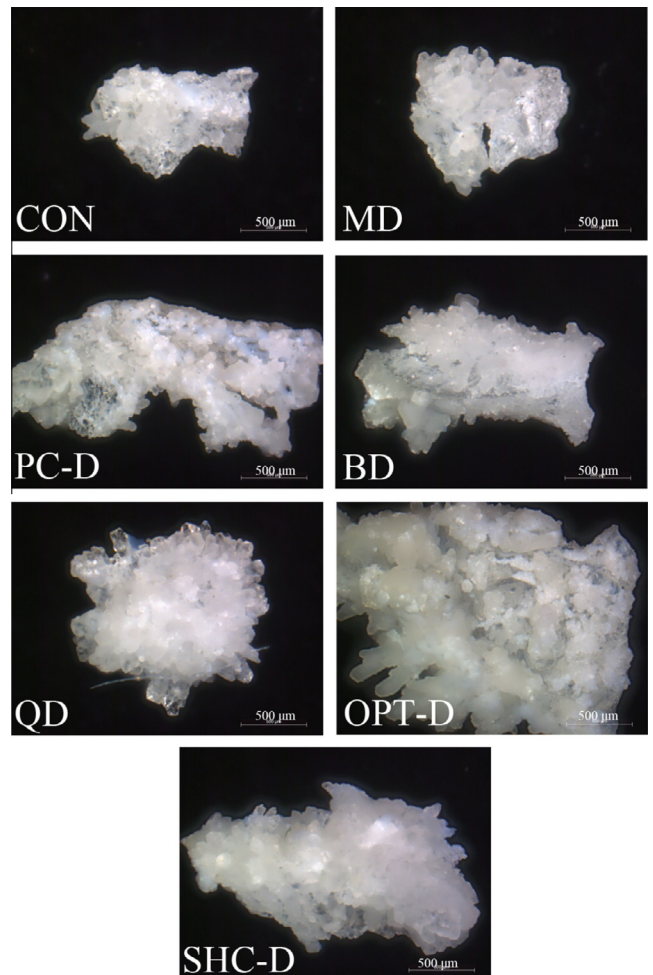


**Fig. 9.** Superficial crack sealing crystal morphology produced in samples crack face.

the perimeter of the cracks as well as their complex crystal structure may have attributed in the durability improvement which is discussed in a subsequent section.

#### 4.2.1. Fourier transform infrared spectroscopy (FT-IR)

The performed FT-IR spectra analysis graph is presented in Fig. 10 to gain insight into the nature of the healing materials micro-structure. As it was mentioned earlier, all healing products were collected from the crack planes of the samples cured under water, specific infrared bands were observed regardless of the types of expansive minerals used.

Along other transmittance bands, sharp bands around  $1424\text{--}1430\text{ cm}^{-1}$  and  $870\text{ cm}^{-1}$  confirmed the presence of carbonate phases ( $\text{--CO}_3$ ) in all samples which were similar with the findings of [27,28]. There was a shallow wide transmittance band around  $3600\text{ cm}^{-1}$  was assigned to  $\text{H--O--H}$  stretching mode of portlandite  $\text{Ca(OH)}_2$ , and  $\text{Mg(OH)}_2$  which could be less dominant due to the samples preservation under acetone for longer period. Sulfate ( $\text{--SO}_4^{2-}$ ) stretching vibrations around  $1116$  and  $1118\text{ cm}^{-1}$  were found in all samples where MD healing samples showed stronger response and similar findings reported by [29,30]. A deep bending around  $980\text{ cm}^{-1}$  was found for the silica ( $\text{Si--O}$ ) bonding presence in all healing compounds which was as an indication of  $\text{SiO}_2$  from mortar sand mixed into the sample and the possibilities of C-S-H jennite type materials similar to [31]. This was further confirmed with a sharp intensity around  $794\text{ cm}^{-1}$  as similarly suggested by [32] for typical quartz. Further the features of the stretching band around  $700\text{ cm}^{-1}$  may attribute to  $\text{Si--O--Al/Mg}$  and any tetrahedral sheet bending around  $530\text{ cm}^{-1}$  possibly may indicate the presence of magnesium in the C-S-H gel materials according to [29,33]. However it is hard to predict considering the accuracy and noise of the signals in the lower end of the spectrum. Nonetheless, there is a shift in peaks and shape changes particularly around  $1100\text{--}900\text{ cm}^{-1}$  in samples containing the concentric capsules compared to the control samples. This observation provides an indirect confirmation of the influence of minerals in the formation of self-healing compounds.

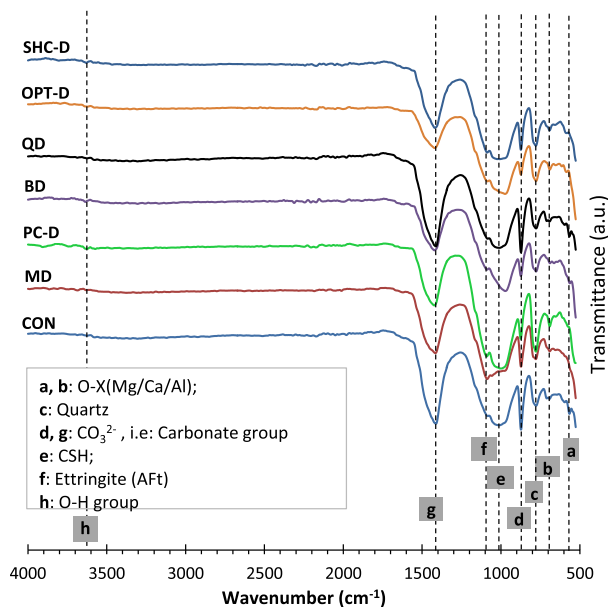


Fig. 10. FTIR spectra of the healing products developed in specimens healed in immersed condition.

#### 4.2.2. XRD analysis on self-healing materials

Fig. 11 shows the XRD patterns for the different healing materials collected from the crack faces of the samples, where most of the peaks are common to all samples. However some characteristic differences for each sample were observed especially with respect to the intensity of the measured peaks. Commonly calcite and silica along with cement rehydrated products such as portlandite ( $\text{Ca(OH)}_2$ ), calcium with silicon and sulfate phases (C-S-H and Ettringite) and primary magnesium hydration phases brucite ( $\text{Mg(OH)}_2$ ) peaks were detected in the XRD with different intensities. Furthermore the common peaks for dicalcium and tricalcium silicate phases ( $\text{C}_2\text{S}$  and  $\text{C}_3\text{S}$ ) were also identified. The presence of calcite in all mixes was obvious as already described in the previous section (Fig. 10), a preponderance of XRD and FT-IR experimental evidence now indicates the calcite crystals precipitation in the peripheral zone. Hence the major calcite intensity at  $\sim 30^\circ$  was found dominant in QD, OPT-D following with BD and MD as quicklime showed more influence on portlandite formation which transformed into calcite with the process of time. The other common dominant peak for silica was due to the sand grain which was accumulated along with cementing self-healing products during collection from healed surface. This may not have influence on the rehydrated self-healing product formation and rather could be considered as a common filling material in healing process in all cases. Comparatively stronger peaks for ettringite were noted in the BD healing products following by QD, OPT-D which could be attributed to the bentonite and quicklime effect on the self-healing materials formation.

Magnesium oxide influence on the MD healing products were found as the strongest intensity for the major brucite peak at  $\sim 18^\circ$  and weaker peaks for different phases of hydrous magnesium carbonate such as dypengite or hydromagnesite ( $\text{MgCO}_3 \cdot 3\text{H}_2\text{O}$ ). There were indications of similar pattern in OPT-D and SHC-D as well, yet the peaks were less observable due to other stronger intensities. These peaks may also indicate the possibility of the hydrous Ca-bearing magnesium carbonate or magnesian calcite formation tendencies in the combined minerals (OPT-D, and SHC-D) healing products. Furthermore, there were possibilities of the presence of hydrotalcite-type phases like  $(\text{Mg}_6\text{Al}_2\text{CO}_3(\text{OH})_{16} \cdot 4\text{H}_2\text{O})$  and calcium magnesium aluminate hydrate  $((\text{C,M})_4\text{AH}_{13})$  as some of the peaks ( $11.5^\circ$ ,  $23^\circ$ ,  $34.5^\circ$  and  $39^\circ$ ) agree with similar observations reported in the literature [34,35], although other stronger intensity of crystalline phases causes their peaks less strong in comparison to others such as  $\text{SiO}_2$ , calcite etc. In closing this section, it is noted that the XRD overlapping intensities and FT-IR observations indicate the apparent complexity of self-healing products formation due to different nature of the encapsulated minerals; this will be further discussed in the SEM imaging and EDX quantification analysis section.

#### 4.2.3. SEM and EDX analysis on self-healing materials formation

Figs. 12 and 13 show the typical SEM images and EDX element detection in each type of self-healed surface. The microstructural observation clearly suggests that the encapsulated minerals were released into the crack successfully. This was evident through the detection of respective hydration and carbonation products formed with the aid of water and  $\text{CO}_2$  (atmospheric and dissolved).

Healing substances were mostly composed of Ca, Si, Al and Mg hydrated and carbonated products. Control and PC-D samples resulted mostly in the formation of Ca-rich products on the self-healing surface such as calcite, portlandite and C-S-H. In all other samples results showed considerable formation of Mg-rich products such as brucite, dypengite/hydromagnesite and Mg-rich calcite (Figs. 12 and 13). Similar dypengite/hydromagnesite (flower-like) microstructural appearance was reported by [36]. The formation of these products can be the result of the reactions in Eqs. (7) and (8), following the initial reaction (Eq.2) presented for brucite formation:



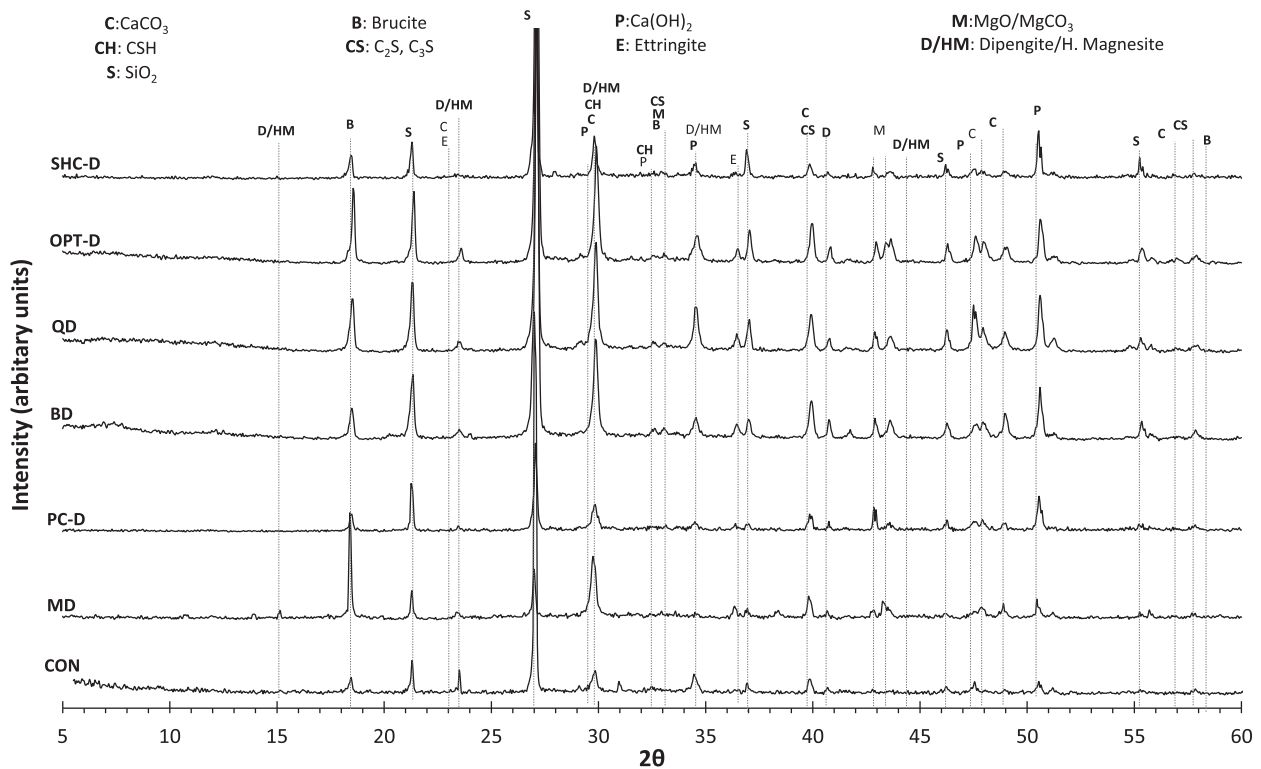
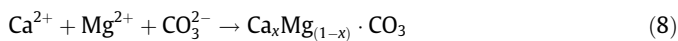
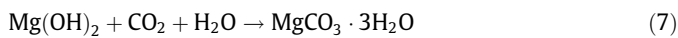


Fig. 11. XRD diffractograms of the self-healing compounds produced in immersed curing condition.



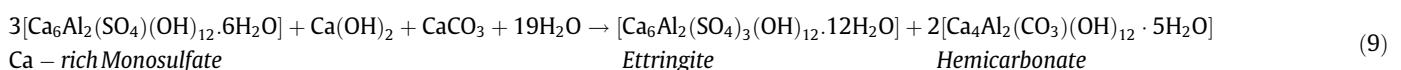
In addition MgO could be responsible to the formation of hydro-talcite type hydrated compounds with the incorporation of silicon and aluminium nuclei in the microstructures as in SHC-D (Fig. 13). Bentonite samples (BD) were found to influence the formation of Al-rich hydro-talcite and aluminate hydrates, such as ettringite compounds on the healing surface. Bentonite was further reported by the Yamaguchi et al. [37] to produce brucite and amorphous silica by conserving aluminium in the high pH sodium hydroxide environment. There is a possibility of similar reactions in the presence of  $\text{Ca}(\text{OH})_2$  into the highly alkaline cement based systems. This brucite and silica producing potential of bentonite can be very beneficial for the production of self-healing compounds.

The samples containing capsules with combination of minerals (OPT-D and SHC-D) as well as the samples with quicklime (QD) resulted in a formation of more self-healing materials compared to samples containing capsules with individual minerals (Fig. 13). The healing potential of combined minerals has been shown in the literature [38], where minerals were used as supplementary materials in concrete samples. Spreading of quicklime in the crack surface distinctively improves portlandite, calcite, C-S-H and even the ettringite production on the self-healing surface. The ettringite formation from the quicklime may be described by the following reaction in Eq. (9) below:

The remaining unhydrated cement in the mortar, tricalcium silicate ( $\text{C}_3\text{S}$ ) and tricalcium aluminate ( $\text{C}_3\text{A}$ ) have also contributed in the formation of portlandite, calcite, calcium silicate hydrate, calcium alumina monosulfate as re-hydration product in all mixes. This triggers autogenous self-healing in the control samples and assists in the healing of other encapsulated mineral systems. However, the microstructure of these re-hydrated products may not be dense enough as it would have been in the case of fresh cement or released minerals.

Fig. 14 shows the ternary diagrams of Ca–Al–Si and Ca–Mg–Si used for the quantitative microstructural analysis of the formed self-healing materials. Normalised values of the EDX detected atomic mass percentage were plotted in the ternary diagram along with some typical SEM images of those detected spots.

As already described in the SEM imaging section the common self-healing compounds were calcite, portlandite and C-S-H which can be spotted in the ternary diagram with typical microstructural morphology. Samples collected from the outer periphery of the crack planes were typically more carbonate rich compounds as shown in Fig. 8. This was further evident from the SEM images (Carbonate rich zone: example SEM images in Fig. 14a and c) with their corresponding EDX atomic mass percentage composition. The impact of MgO in the MD, OPT-D and SHC-D healing surface was evidenced by the existence of Mg-rich compounds. Similarly bentonite influenced in the formation of Al, Si and Mg rich compounds (Fig. 14). The self-healing gel/amorphous materials with lower Ca/Si (Ca/Si = 1) ratio revealed a sheet like morphology (See Fig. 12 for BD sample) while higher Ca/Si (Ca/Si > 1.3) ratio showed a hazy



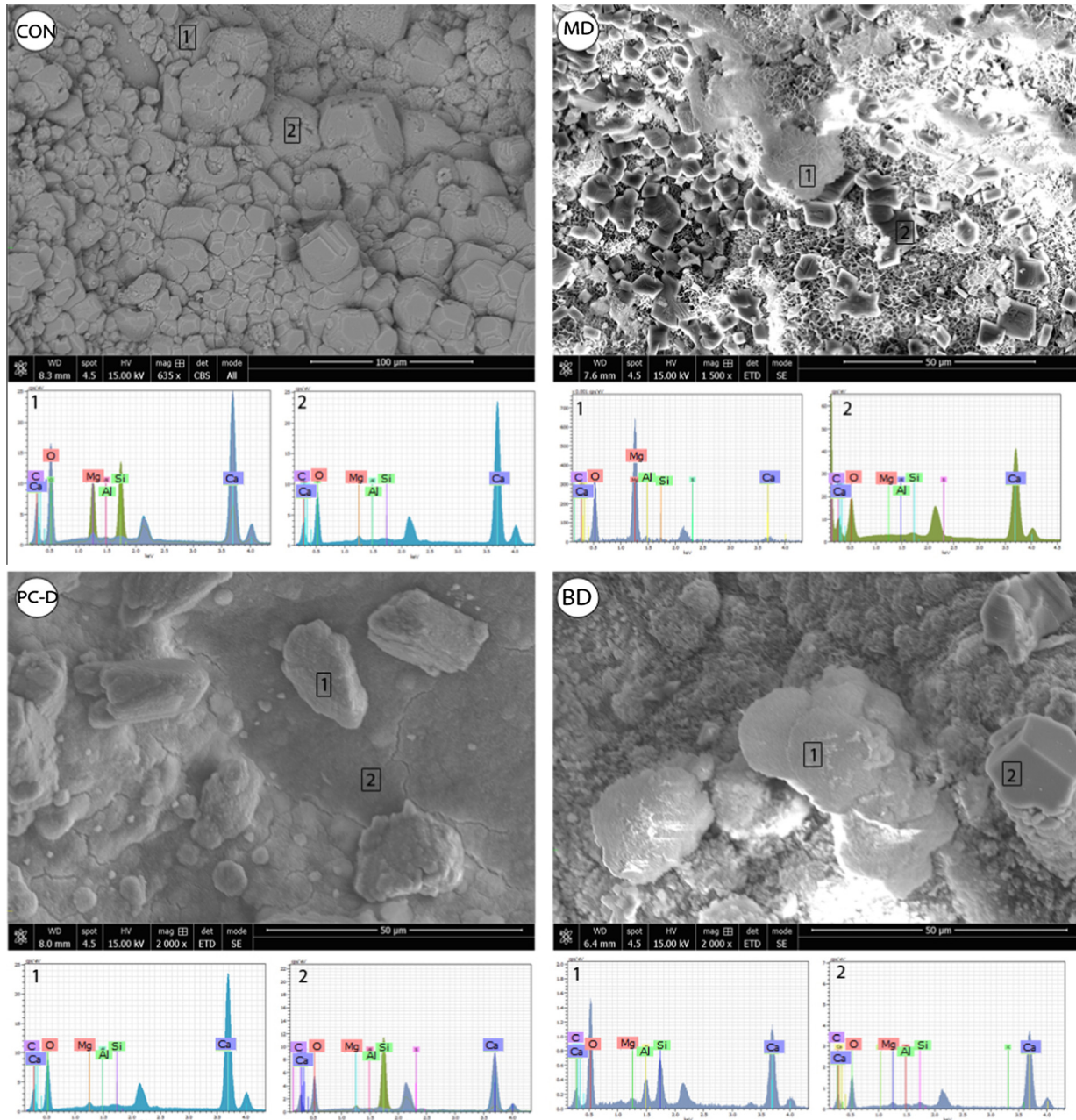


Fig. 12. SEM-EDX images of self-healing crack surface after re-cracking: CON, MD, PC-D, and BD.

fibrillar structure as can be noticed in QD samples (Fig. 12). Similar C-S-H microstructure were discussed by Chiang et al. [39] and Pelisser et al. [40] who have further suggested that at higher Ca/Si ratio, it is hard for the C-S-H micro-structure to be more planar resulting in a continuous morphology at a larger length-scale. The observed micro-structural morphology of the formed healing material have suggested that the released expansive minerals in the crack zone affected C-S-H gel reducing the extension of the planar structure to more in an open arrangement. This can be possible as Chiang et al. [39] suggests that Ca/Si ratio increment with the addition of methylhydroxyethyl cellulose (Culminal), a commonly used additive in the cement industry, can enlarge the fractal domain resulting into a similar phenomenon. Even the calcium aluminium silicate hydrate (CASH) appeared into higher Ca-rich zone suggests an arrangement of  $C_{1.94}A_{0.96}SH_x$  similar to one

reported in the literature [41]. Some products also showed very close atomic combination such as magnesium silicate hydrates with lower Ca proportions in MD samples. Hence three common Mg-rich minerals such as bredigite ( $Ca_7Mg(Si_2O_4)_4$ ), monticellite ( $CaMgSiO_4$ ) [29] and dolomite ( $CaMg(CO_3)_2$ ) were plotted in the ternary diagrams for comparative purposes. It could be noted that few healing compounds have similar atomic mass percentages as of bredigite and monticellite. However products with  $Mg/Ca \approx 0.25-0.5$  in ternary plots indicate magnesian calcite. The ratio  $Mg/Ca > 0.5$  can be an indication for the formation of brucite, hydromagnesite and even hydrocalcite. Magnesium rich compounds were found in the MD and combined minerals samples. In closing this section, it has to be highlighted that the formation of additional hydrated products, due to the fracture of the concentric capsules, was beneficial for the healing of the formed cracks.

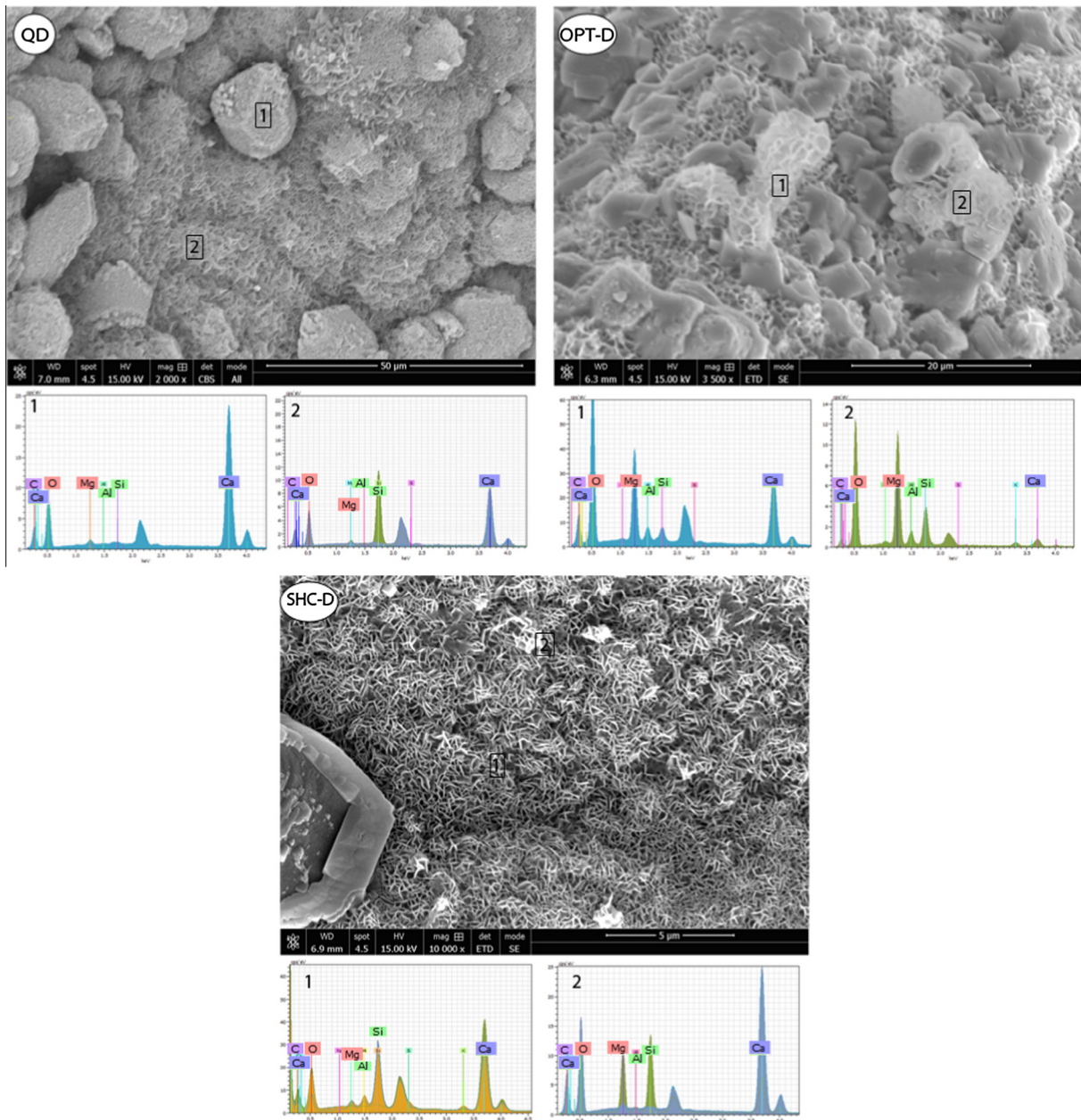


Fig. 13. SEM-EDX images of self-healing crack surface after re-cracking: QD, OPT-D, and SHC-D.

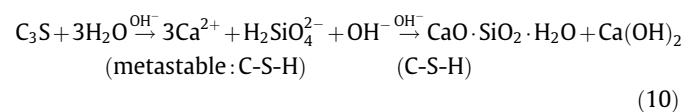
The data analysis so far shows that the combined minerals were found more efficient compared to capsules containing individual mineral.

#### 4.3. Kinetics of the Self-healing with expansive minerals

It is known that impure tricalcium silicate  $\text{Ca}_3\text{SiO}_5$  or  $\text{C}_3\text{S}$  (alite) constitutes about 50%–70% of the PC by mass. Therefore, to simplify the study of the hydration kinetics of PC systems, emphasis is given on the hydration characteristics of  $\text{C}_3\text{S}$ . The microstructural development and solution chemistry during hydration in healing process either follows metastable barrier hypothesis [42,43] or the slow dissolution step hypothesis [44,45] during self-healing materials proliferation.

The healing process accelerated with the autogenous self-healing, which was the hydration of remaining unhydrated  $\text{C}_3\text{S}$  from the surface of the crack. The hydration process after releasing

of minerals was related to the heterogeneous nucleation and growth (N + G) of healing compounds on the crack surfaces such as C-S-H growth on the crack zone. This is similarly evident in cement hydration discussed in the literature [45–50]. During initial re-hydration of PC portion, rapid reaction starts between  $\text{C}_3\text{S}$  and water when  $\text{C}_3\text{S}$  dissolves based on the reaction described with Eq.10 [18]:



However in the encapsulated samples, quicklime in particular and the silicate of bentonite resulted in the formation of more crystalline C-S-H as observed by SEM-EDX (Figs. 12–14). These encapsulated minerals can cause higher supersaturations compared to

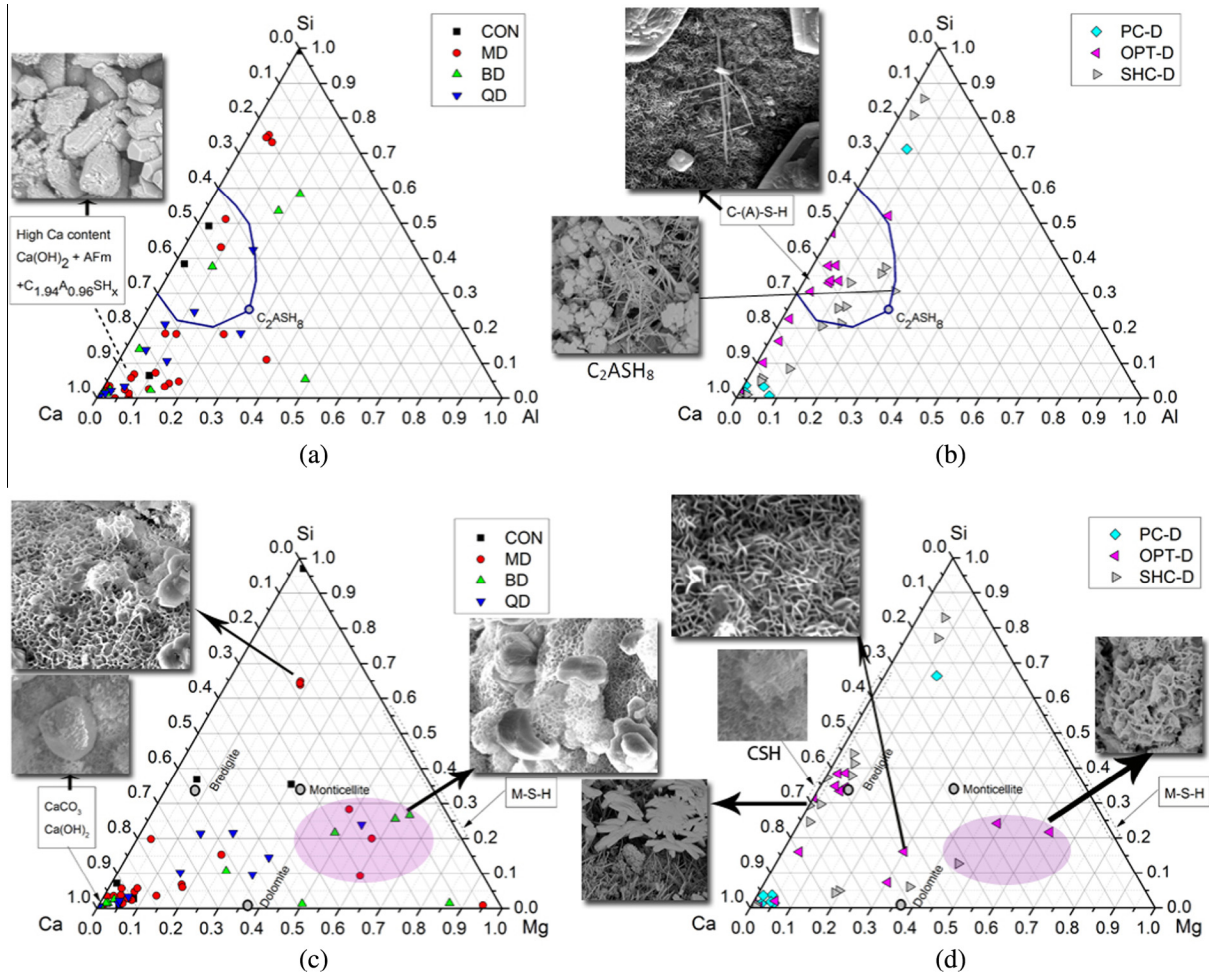


**Fig. 14.** Ternary diagrams EDX material compositions, a. Ca–Al–Si of CON,MD,BD,QD; b. Ca–Al–Si of PC-D,OPT-D,SHC-D; c. Ca–Mg–Si of CON,MD,BD,QD; and d. Ca–Mg–Si of PC-D,OPT-D,SHC-D.

the portlandite thus accelerating the nucleation of portlandite and C–S–H and their growth without dissolving much  $C_3S$ . Similar phenomenon was reported by Bullard et al. [18].

Although direct observations of the first nucleation process for self-healing systems are difficult to perform, the nucleation process in the chemical reaction for self-healing and the isotropic growth of healing products in the crack supports the (N + G) mechanisms. The nucleation of released minerals occurs while threshold of a metastable hydrate layers forms in the crack surface. The hydration products then start precipitating by metastable layer conversion directly or through solution mechanisms. This was the reason of longer time requirement for healing compounds formation as nucleation and growth of compounds requires this pre-existing hydrate phase. Initially just after the ions release on the crack zone, the solution was supersaturated with respect to hydroxides, and ionic concentration drops rapidly after the induction period. For example, the maximum ratio of the calcium ions assisting to the solubility of portlandite (CH) products is about 4.5–5 for the pastes with water to solid ratio  $\sim 1$  at the N + G period of the early age cement hydration suggested by Young et al. [51].

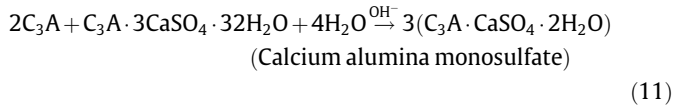
Magnesium oxide from the encapsulation systems initially hydrates to form brucite (MH) which contributes to the formation of different secondary and tertiary products such as hydromagnesite, tetrahedral silicate growing in silicate chains of 2D sheets incorporating magnesium, calcium and hydroxyle between the layers forming a jennite or torbermorite like structures. Nucleation

keeps growing in similar fashion forming well-ordered layers and the crystal structures thickness over time. In all cases after initial N + G period, the active elements of encapsulated expansive minerals such as  $Mg^{2+}$ ,  $Ca^{2+}$ ,  $Al^{3+}$ ,  $Si^{4+}$  further enter inside layer like defects and (mineral ions incorporation) rate increases with the growth of lattice structures. Therefore the growth of hydration products such as C–S–H, CH, MH etc., continuously removed ions form the solution. This process keep continue latter through the further diffusion of unhydrated ions form mineral encapsulations. Similar action of ionic concentration hydration mechanisms was suggested by Bullard et al. [18] while explaining the cement hydration in early stages. Over time the hydration products keep forming and these minerals within the microstructural sheets (C–S–H, CH, MH) cause them to buckle by diverging away from each other. This buckling effect disordered the crystalline structure as evident in the SEM-image of the healed surface (Fig. 12 and 13).

Then again, the reaction rate of  $C_3A$  unlike alite is very fast which results almost instantaneous setting in Portland cement. A poorly crystallised  $Al_2O_3$ – $Fe_2O_3$ – monomer, generally attributed as AFm phases with the formula  $[Ca_2(Al,Fe)(OH)_6]^{x-} \cdot xH_2O$  according to [52] and described as  $C_2AH_8$  and  $C_4AH_{13}$  [53,54], where intercalated layers of these both phases may exist. Hence calcium sulfate is typically added to cement to retard the reaction of  $C_3A$  and control the time of AFm phases. At this stage, ettringite  $[C_3A \cdot 3CaSO_4 \cdot 32H_2O]$  is the main hydration product. The added calcium sulfate delayed the reaction time until it was all consumed

and the reaction accelerated again forming calcium mono sulfoaluminate as the main product phase.

The length of the slow reaction period according to Minard et al. [55] is approximately linear with the amount of calcium sulfate in the cement matrix. Succeeding the consumption of sulfate, second stage dissolution of  $C_3A$  produces calcium aluminium monosulfate following the reaction below:



Expansive materials like MgO, bentonite and quicklime can modify the early hydration rates as similar phenomena were investigated by Thomas et al. [50] while they added a particular nucleating agent in the cement matrix.

In this work, the hydration rate was controlled by a diffusion process, even though three other factors played important role: (i) consumption of small mineral particles at early hydration leaving larger ones to react later; (ii) space limitations after initial hydrated product formation and (iii) limited water availability. Faster hydration and growth of C-S-H micro-structure observed by Constantinides and Ulm [56] was highly porous which attributes in the rehydration process of self-healing. An example of the porous structure for the faster formatted healing compound can be noted in Fig. 14 for  $C_2ASH_8$ . However, the packing density of the hydrated products might be initially lower and it increase with time. Finally major portion of active hydrated products had carbonated as far the dissolved and atmospheric  $CO_2$  could be reached which have resulted calcite and other carbonate products formation in the samples periphery zone (Fig. 8). Therefore the crystal growth and nucleation in the crack surface formed effective bridging with the precipitated hydrated products of capsule minerals thus healing the crack.

#### 4.4. Capillary sorption

Fig. 15 shows the measured sorptivity coefficients for all samples after 28 days of healing. The results were benchmarked against an uncracked control sample (CON-UN). Following the results discussed earlier on load regain and CA%, since the immersed specimens found to exhibit the best healing performance; it was only this type of specimens used for sorptivity measurements. The efficient dispersion of minerals samples with capsules had resulted in remarkable improvement in the sorptivity coefficient compared to the control cracked (CON-CR) samples. The

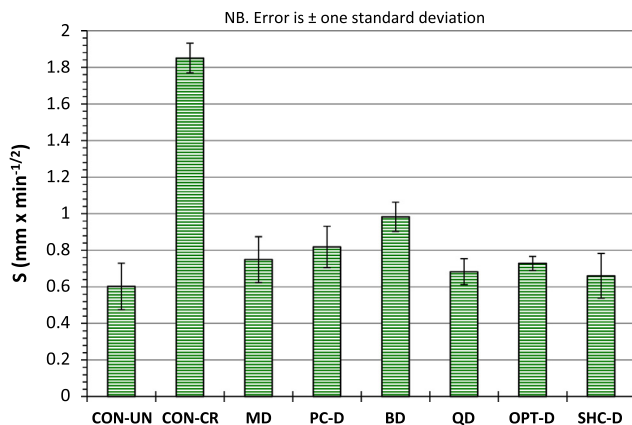


Fig. 15. Coefficient of sorptivity for all samples healed under immersed in water condition.

largest reduction of the capillary absorption compared to CON-cracked samples were measured for SHC-D, QD, OPT-D and MD about 64 ~ 60%. In fact these four types of specimens exhibited a performance that compares very well with the control uncracked samples. Therefore, the encapsulated minerals in these occasions managed to restore the sorptivity coefficients close to the level of undamaged samples. However, individual minerals, bentonite and PC, showed the least reduction in the sorptivity coefficient compared to the control cracked samples resulting in a reduction of about 47% and 55% respectively. Overall findings are not too different from the mechanisms proposed in the previous findings with liquid minerals [4]. In addition, the use of the concentric glass capsules showed significant improvement in the sorptivity measurements compared to the encapsulation of MgO powder using the parallel glass capsules [4]. In the parallel tube system the sorptivity reduction of the samples containing powder minerals was 46% with respect to the control specimens. Therefore, the concentric capsules system improved the sorptivity reduction by almost 20%.

While capsules containing samples have resulted in considerable reduction of the sorptivity coefficient compared to control samples, macroscopic observations during tests have further validated the findings. The significant reduction in the water uptake is a strong indication that the life expectancy of the cracked sections containing the concentric capsule system will be substantially improved compared to the non-containing ones. The capillary sorption tests also indicate that the healing deep inside the crack is more extensive for the samples with the concentric capsules. The surface crack measurements shown in Fig. 4 revealed a small difference between control and the rest of the samples. However, capillary absorption test clearly demonstrated the importance of the proposed system as the permeability regain compared to the control samples was substantial. Fig. 16 presents three typical cases where water sorption and diffusion vary between control samples and samples containing capsules. Specifically CON samples absorb more water followed by BD samples (Fig. 16b) and SHC-D samples (Fig. 16c) which absorb the least. Their corresponding sorptivity coefficients, illustrated in Fig. 15, showed similar trend. Although BD sample (Fig. 16b) seems to absorb a significant amount of water this could be attributed to the high water absorption properties of bentonite clay. In addition since bentonite is not as reactive as the other minerals (MgO and CaO) its hydration products are not as dense as in the other combinations. As a result, although the cracks closed by the bentonite hydration products (see Fig. 5), these seem to be more permeable

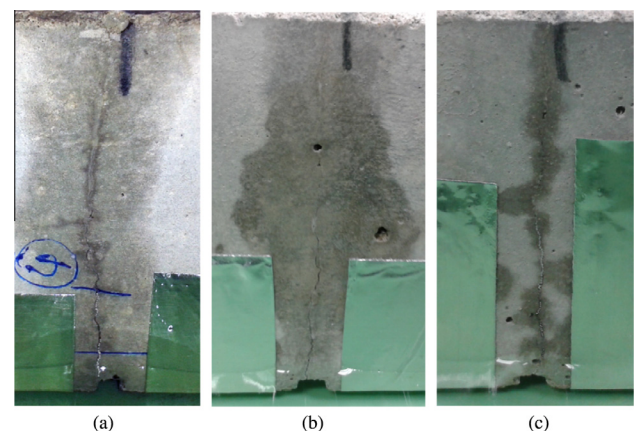


Fig. 16. Sorptivity test indication for durability concern, image taken after 2 h of running the test: (a) Control cracked; (b) Less-water tight although smaller crack width indicating comparatively less durability increment (eg. MB); (c) More-water tight indicating increasing durability (eg. SHC-D).

than the healing products formed in the other combinations. The CON and PC capsule systems may have resulted in the formation of thin layers of calcite crystals in the vicinity of the crack tip. This has resulted to some crack sealing but the mechanical strength recovery and sorptivity performance after healing were restricted.

In few cases, CON and BD samples shows thin layers of superficial crack sealing due to the formation of calcite in crack tip and porous healing compounds such as ettringite inside. This was also indicated by micro-structural investigation of the self-healing materials in associated samples. Hence these healed samples accordingly resulted in higher sorptivity coefficient indicating less durability improvement. Although, quicklime was found to encourage ettringite formation in the early stages of the self-healing (Eq.9), portlandite, calcite and C-S-H keep growing within the ettringite structure leading to continuous proliferation of the healing compounds within the crack thus improved durability. Similarly MgO and combined minerals (OPT-D and SHC-D) were initially healed through formation of metastable healing layers and proliferation of healing products over time as explained in the self-healing kinetics and micro-structure section. The overall self-healing process was studied by detailed microstructural investigation of the formed self-healing materials and the associated cement hydration kinetics. However further knowledge is needed for each stage of controlling reaction in the dissolution and the nucleation and growth of each hydration products phase. A complete description would also include the temperature dependence of the self-healing process.

The proposed system of concentric glass capsules showed that it can improve the self-healing capacity of mortars in all cases of minerals used. However, the combination of minerals resulted in an efficient healing and had more consistent performance throughout all experimental procedures undertaken in this study. These results have substantiated the potential of the expansive minerals for the concrete autonomic self-sealing applications which in future also could be extended to the use of pellets made of expansive minerals or even in the microencapsulation of powder minerals.

## 5. Conclusions

This study investigated the self-healing behaviour of expansive minerals while encapsulated in a system of concentric glass macro-capsules and embedded into the cement mortar matrix. It was focused on securing a better understanding of particular expansive minerals influence on self-healing mechanisms, and the physics and chemistry of the hydration kinetics. Encapsulated expansive minerals (MgO, bentonite and quicklime) were used individually and in combination and their self-healing performance were compared in terms of load recovery, crack sealing and capillary water absorption. Combined minerals showed most consistence self-healing performance followed by samples containing encapsulated PC, MgO, quicklime, bentonite and control samples. The technical findings of the paper could be summarised as below:

1. Unhydrated minerals presents in the crack surface and releases from the capsules take part in the re-hydration process for the self-healing.
2. Self-healing hydration kinetics follows the hydrokinetic steps described in the literature section. This was comprised of the dispersion and dissolution of expansive minerals then nucleation and growth of hydrating healing compounds following complexation, diffusion control and adsorption stages.
3. The initial proliferation of the  $\text{Ca}(\text{OH})_2$  and  $\text{Mg}(\text{OH})_2$  seems to result in the formation of a denser healing compounds. Formation of denser ionic layers starts hydrating with the presence of water leading a faster decrease of crack volume.

4. Initially hydration products such as  $\text{Ca}(\text{OH})_2$ ,  $\text{Mg}(\text{OH})_2$ , C-S-H, and aluminosilicate hydrates form and expand in the crack voided zone.
5. Over time,  $\text{CO}_2$  (atmospheric or dissolved in water) reacts with reactive hydrating products forming various carbonates and hydro-carbonates. A more crystalline type products layers start forming in crack periphery until it had sealed the crack which was observed by macroscopic and microstructural investigation.
6. Densification of healing layers enhanced with the presence of more unreacted ions in the cracks. Crack bridging occurs by the effective formation of healing compounds in the crack zone which not only have caused effective crack sealing resulting improvement in durability, but also have considerably improved mechanical strength.
7. Finally it is very important to highlight the fact that the proposed concentric glass capsules system found to be very effective in closing very large cracks at sizes that according to the design standards are in the boundary of being acceptable ( $\sim 400 \mu\text{m}$ ).

## Acknowledgement

The support of Islamic Development Bank (IDB) scholarship collaborating with Cambridge Overseas Trust for the first author's PhD research is greatly appreciated. Moreover, financial support from the Engineering and Physical Sciences Research Council (EPSRC) for this study (Project Ref. EP/K026631/1 – “Materials for Life”) is also gratefully acknowledged.

Additional data related to this publication is available at the University of Cambridge's institutional data repository: <https://www.repository.cam.ac.uk/handle/1810/254442>.

## References

- [1] M. Rooij, K. van Tittelboom, N. Belie, E. Schlangen (Eds.), Self-Healing Phenomena in Cement-Based Materials: State-of-the-Art Report of RILEM Technical Committee 221-SHC: Self-Healing Phenomena in Cement-Based Materials, Springer, 2013.
- [2] H.-W. Reinhardt, M. Jooss, Permeability and self-healing of cracked concrete as a function of temperature and crack width, *Cem. Concr. Res.* 33 (7) (2003) 981–985, Jul.
- [3] K. Van Tittelboom, N. De Belie, Self-Healing in Cementitious Materials, *A Review* 6 (6) (2013).
- [4] A. Kanellopoulos, T.S. Qureshi, A. Al-Tabbaa, Glass encapsulated minerals for self-healing in cement based composites, *Constr. Build. Mater.* 98 (Nov. 2015) 780–791.
- [5] V. Li, E. Yang, Self healing in concrete materials, self heal. Mater. An Altern. Approach to 20 Centuries, *Mater. Sci.* 100 (2007) 161.
- [6] C. Joseph, A.D. Jefferson, B. Isaacs, R. Lark, D. Gardner, Experimental investigation of adhesive-based self-healing of cementitious materials, *Mag. Concr. Res.* 62 (11) (Nov. 2010) 831–843.
- [7] V.C. Li, Y.M. Lim, Y.-W. Chan, Feasibility study of a passive smart self-healing cementitious composite, *Compos. Part B Eng.* 29 (6) (Nov. 1998) 819–827.
- [8] C.M. Dry, Design of self-growing, self-sensing, and self-repairing materials for engineering applications, in: *Proceedings of SPIE – The International Society for Optical Engineering*, 2001, pp. 23–29.
- [9] H. Mihashi, Y. Kaneko, T. Nishiwaki, K. Otsuka, Fundamental study on development of intelligent concrete characterized by self-healing capability for strength, *Trans. Japan Concr. Inst.* 22 (Feb. 2001) 441–450.
- [10] C. Dry, W. McMillan, Three-part methylmethacrylate adhesive system as an internal delivery system for smart responsive concrete, *Smart Mater. Struct.* 5 (3) (Jun. 1996) 297–300.
- [11] K. Van Tittelboom, N. De Belie, D. Van Loo, P. Jacobs, Self-healing efficiency of cementitious materials containing tubular capsules filled with healing agent, *Cem. Concr. Compos.* 33 (4) (Apr. 2011) 497–505.
- [12] M.M. Pelletier, R. Brown, A. Shukla, A. Bose, Self-healing concrete with a microencapsulated healing agent, no. C, 2011.
- [13] T. Qureshi, A. Al-Tabbaa, The effect of magnesia on the self-healing performance of Portland cement with increased curing time, 1st International Conference on Ageing of Materials & Structures, 2014, pp. 635–642.
- [14] K. Sisomphon, O. Copuroglu, E.A.B. Koenders, Self-healing of surface cracks in mortars with expansive additive and crystalline additive, *Cem. Concr. Compos.* 34 (4) (2012) 566–574, Apr.

- [15] T.-H. Ahn, T. Kishi, Crack self-healing behavior of cementitious composites incorporating various mineral admixtures, *J. Adv. Concr. Technol.* 8 (2) (2010) 171–186.
- [16] T. Qureshi, A. Al-Tabbaa, Self-healing of drying shrinkage cracks in cement-based materials incorporating reactive MgO, *Smart Mater. Struct.* (2016), vol. [in press].
- [17] L. Sanchez, J. Cuevas, S. Ramirez, D. Riuizdeleon, R. Fernandez, R. Vigildelavilla, S. Leguey, Reaction kinetics of FEBEX bentonite in hyperalkaline conditions resembling the cement–bentonite interface, *Appl. Clay Sci.* 33 (2) (Jul. 2006) 125–141.
- [18] J.W. Bullard, H.M. Jennings, R.A. Livingston, A. Nonat, G.W. Scherer, J.S. Schweitzer, K.L. Scrivener, J.J. Thomas, Mechanisms of cement hydration, *Cem. Concr. Res.* 41 (12) (Dec. 2011) 1208–1223.
- [19] P.M. Dove, N. Han, J.J. De Yoreo, Mechanisms of classical crystal growth theory explain quartz and silicate dissolution behavior, *Proc. Nat. Acad. Sci. U.S.A.* 102 (43) (Oct. 2005) 15357–15362.
- [20] A.W. Adamson, A.P. Gast, *Physical Chemistry of Surfaces*, 6th ed., Wiley-Interscience, New York, 1997.
- [21] D. Kashchiev, G.M. Van Rosmalen, Review: nucleation in solutions revisited, *Cryst. Res. Technol.* 38 (7–8) (2003) 555–574.
- [22] W.K. Burton, N. Cabrera, F.C. Frank, The growth of crystals and the equilibrium structure of their surfaces, *Philos. Trans. R. Soc. A Math. Phys. Eng. Sci.* 243 (866) (Jun. 1951) 299–358.
- [23] W. Stumm, J.J. Morgan, *Aquatic Chemistry*, Wiley-Interscience, New York, 1972.
- [24] M. Shand, *The Chemistry and Technology of Magnesia*, 2006.
- [25] C.K. Chau, Z. Li, Accelerated reactivity assessment of light burnt magnesium oxide, *J. Am. Ceram. Soc.* 91 (23712) (2008) 1640–1645.
- [26] J. Kropp, RILEM Technical committees RILEM TC 116-PCD : permeability of concrete as a criterion of its durability recommendations, test for gas permeability of concrete a preconditioning of concrete test specimens for the measurement of gas permeability and capilar, *Mater. Struct.* 32 (April) (1999) 174–179.
- [27] M. Trezza, A. Lavat, Analysis of the system  $3\text{CaO} \cdot \text{Al}_2\text{O}_3 \cdot \text{CaSO}_4 \cdot 2\text{H}_2\text{O} \cdot \text{CaCO}_3 \cdot \text{H}_2\text{O}$  by FT-IR spectroscopy, *Cem. Concr. Res.* (2001).
- [28] P. Yu, R. Kirkpatrick, Structure of calcium silicate hydrate (C-S-H): Near-, Mid-, and Far-infrared spectroscopy, *J. Am. Ceram. Soc.* 82 (3) (1999) 742–748.
- [29] L. Fernandez, C. Alonso, C. Andrade, A. Hidalgo, The role of magnesium during the hydration of C3S and C-S-H formation. Scanning electron microscopy and mid-infrared studies, *Adv. Cem. Res.* 17 (1) (2005) 9–21.
- [30] R. Ylmén, U. Jäglid, B.M. Steenari, I. Panas, Early hydration and setting of Portland cement monitored by IR, SEM and Vicat techniques, *Cem. Concr. Res.* 39 (5) (2009) 433–439.
- [31] F. Kontoleonos, P. Tsakiridis, Dry-grinded ultrafine cements hydration. physicochemical and microstructural characterization, *Mater* (2013).
- [32] D. Alves Fungaro, M. Valério da Silva, Utilization of water treatment plant sludge and coal fly ash in brick manufacturing, *Am. J. Environ. Prot.* 2 (5) (Oct. 2014) 83–88.
- [33] A.A. Reddy, A. Goel, D.U. Tulyaganov, S. Kapoor, K. Pradeesh, M.J. Pascual, J.M.F. Ferreira, Study of calcium–magnesium–aluminum–silicate (CMAS) glass and glass-ceramic sealant for solid oxide fuel cells, *J. Power Sources* 231 (Jun. 2013) 203–212.
- [34] J.I. Escalante-García, A.F. Fuentes, A. Gorokhovskiy, P.E. Fraire-Luna, G. Mendoza-Suarez, Hydration products and reactivity of blast-furnace slag activated by various alkalis, *J. Am. Ceram. Soc.* 86 (12) (Dec. 2003) 2148–2153.
- [35] S. Song, H. Jennings, Pore solution chemistry of alkali-activated ground granulated blast-furnace slag, *Cem. Concr. Res.* 29 (2) (1999) 159–170.
- [36] S. Teir, S. Eloneva, C.J. Fogelholm, R. Zevenhoven, Fixation of carbon dioxide by producing hydromagnesite from serpentinite, *Appl. Energy* 86 (2) (2009) 214–218.
- [37] T. Yamaguchi, Y. Sakamoto, M. Akai, M. Takazawa, T. Tanaka, S. Nakayama, T. Sato, Experimental study on dissolution of montmorillonite in compacted sand-bentonite mixture under Na-Cl-OH pore-water conditions, *Proceedings of Joint NUMO-Posiva International Workshop on Bentonite-Cement Interaction in Repository Environments*, 2004, pp. 125–131.
- [38] Z. Jiang, W. Li, Z. Yuan, Influence of mineral additives and environmental conditions on the self-healing capabilities of cementitious materials, *Cem. Concr. Compos.* 57 (Mar. 2015) 116–127.
- [39] W.-S. Chiang, G. Ferraro, E. Fratini, F. Ridi, Y.-Q. Yeh, U.-S. Jeng, S.-H. Chen, P. Baglioni, Multiscale structure of calcium- and magnesium-silicate-hydrate gels, *J. Mater. Chem. A* 2 (32) (Jul. 2014) 12991.
- [40] F. Pelisser, P.J.P. Gleize, A. Mikowski, Effect of the Ca/Si Molar Ratio on the Micro/nanomechanical Properties of Synthetic C-S-H Measured by Nanoindentation, *J. Phys. Chem. C* 116 (32) (Aug. 2012) 17219–17227.
- [41] I. Garcia-Lodeiro, A. Palomo, A. Fernández-Jiménez, D.E. Macphée, Compatibility studies between N-A-S-H and C-A-S-H gels. Study in the ternary diagram  $\text{Na}_2\text{O}-\text{CaO}-\text{Al}_2\text{O}_3-\text{SiO}_2-\text{H}_2\text{O}$ , *Cem. Concr. Res.* 41 (9) (Sep. 2011) 923–931.
- [42] E.M. Gartner, J.M. Gaidis, Hydration mechanisms: I, *Hydration Mech.* III 1 (1989) 95–125.
- [43] H.M. Jennings, P.L. Pratt, An experimental argument for the existence of a protective membrane surrounding portland cement during the induction period, *Cem. Concr. Res.* 9 (4) (Jul. 1979) 501–506.
- [44] D. Damidot, F. Bellmann, B. Möser, T. Sovoidnich, Calculation of the dissolution rate of tricalcium silicate in several electrolyte compositions, *Cem. Wapno Bet.* 2 (2007) 57–67.
- [45] S. Garrault, E. Finot, E. Lesniewska, A. Nonat, Study of C-S-H growth on C3S surface during its early hydration, *Mater. Struct.* 38 (4) (May 2005) 435–442.
- [46] E.M. Gartner, J.F. Young, D.A. Damidot, I. Jawed, Hydration of portland cement, in: J. Bensted, P. Barnes (Eds.), *Structure and Performance of Cements*, 2nd ed., Spon Press, New York, 2002, pp. 57–113.
- [47] S. Garrault, A. Nonat, Hydrated layer formation on tricalcium and dicalcium silicate surfaces: experimental study and numerical simulations, *Langmuir* 17 (26) (Dec. 2001) 8131–8138.
- [48] J.J. Thomas, A new approach to modeling the nucleation and growth kinetics of tricalcium silicate hydration, *J. Am. Ceram. Soc.* 90 (10) (Oct. 2007) 3282–3288.
- [49] S. Bishnoi, K.L. Scrivener,  $\mu\text{ic}$ : A new platform for modelling the hydration of cements, *Cem. Concr. Res.* 39 (4) (Apr. 2009) 266–274.
- [50] J.J. Thomas, H.M. Jennings, J.J. Chen, Influence of nucleation seeding on the hydration mechanisms of tricalcium silicate and cement, *J. Phys. Chem. C* 113 (11) (Mar. 2009) 4327–4334.
- [51] J.F. Young, H.S. Tong, R.L. Berger, Composition of solutions in contact with hydrating tricalcium silicate pastes, *J. Am. Ceram. Soc.* 60 (5–6) (1977) 193–198.
- [52] E. Gallucci, P. Mathur, K. Scrivener, Microstructural development of early age hydration shells around cement grains, *Cem. Concr. Res.* 40 (1) (Jan. 2010) 4–13.
- [53] H.F.W. Taylor, *Cement Chemistry*, Thomas Telford, 1997.
- [54] W.A. Corstanje, H.N. Stein, J.M. Stevels, Hydration reactions in pastes  $\text{C}_3\text{S} + \text{C}_3\text{A} + \text{CaSO}_4 \cdot 2\text{aq} + \text{H}_2\text{O}$  at 25 °C, *Cem. Concr. Res.* 4 (1974) 417–431.
- [55] H. Minard, S. Garrault, L. Regnaud, A. Nonat, Mechanisms and parameters controlling the tricalcium aluminate reactivity in the presence of gypsum, *Cem. Concr. Res.* 37 (10) (Oct. 2007) 1418–1426.
- [56] G. Constantinides, F.-J. Ulm, The nanogranular nature of C-S-H, *J. Mech. Phys. Solids* 55 (1) (Jan. 2007) 64–90.